JOURNAL OF SOLID STATE CHEMISTRY 31, 135–143 (1980)

Subsolidus Phase Diagram of Cu_2O–CuO–MoO_3 System

TADEUSZ MACHEJ AND JACEK ZIÓŁKOWSKI

Research Laboratories of Catalysis and Surface Chemistry, Polish Academy of Sciences, Krakow, Poland

Received August 29, 1978, in revised form January 28, 1979

Five chemical compounds, $CuMoO_4$, $Cu_3Mo_2O_9$, $Cu_2Mo_3O_{10}$, $Cu_6Mo_4O_{15}$, and $Cu_{4-x}Mo_3O_{12}$ ($0.10 \leq x \leq 0.40$), were identified in the system Cu_2O–CuO–MoO_3 and characterized by DTA, X-ray powder patterns, ir spectra, and magnetic properties. Cupric molybdates $CuMoO_4$ and $Cu_3Mo_2O_9$ are stable in air up to 820 and 855°C, respectively, melting at these temperatures with simultaneous decomposition (oxygen loss). Congruent mp of cuprous molybdates $Cu_2Mo_3O_{10}$ and $Cu_6Mo_4O_{15}$, in argon, are 532 and 466°C, respectively. Nonstoichiometric phase $Cu_{4-x}Mo_3O_{12} = Cu_3^{2+}Cu_{1-x}^{0}Mo_3^{6+}O_{12}$, melts in argon between 630 and 650°C depending on the value of x and at 525–530°C undergoes polymorphic transformation. Areas of coexistence of the above-mentioned phases are determined. The μ_{eff} of Cu^{2+} ions and θ values are: 1.80 B.M. and 28°K for $CuMoO_4$, 1.71 B.M. and −12°K for $Cu_3Mo_2O_9$, and 1.74 B.M. and −93°K for $Cu_{4-x}Mo_3O_{12}$. Below 200°K $CuMoO_4$ becomes antiferromagnetic. $Cu_2Mo_3O_{10}$ and $Cu_6Mo_4O_{15}$ show weak temperature-independent paramagnetism.

Introduction

The literature on the CuO–MoO_3 system describes three cupric molybdates: $CuMoO_4$ (*1–9*), $Cu_3Mo_2O_9$ (*5, 8, 10–12*), and Cu_2MoO_5 (*4, 8, 9*). According to the most detailed paper on this subject, published by Nassau and Shiever (*8*), all these salts when heated in air melt incongruently between 800 and 850°C and slightly above melting temperature decompose with evolution of oxygen. It has been, however, a matter of controversy whether $Cu_3Mo_2O_8$ (*10*), $Cu_{4-x}Mo_3O_{12}$, with $x \approx 0.15$ (*13*), $Cu_6Mo_4O_{15}$ (*4, 8*), or $Cu_2Mo_3O_x$ (*14*) are the solid products of decomposition. At any rate, the oxygen loss results in movement from the CuO–MoO_3 to the Cu_2O–MoO_3 system and brings about some phase diagram inconsistencies, reviewed in (*8*) and never entirely cleared up until now.

It should be stressed that there are only a few data useful for undoubtful identification of phases in the Cu_2O–CuO–MoO_3 system. The structures have been resolved for only three compounds, $CuMoO_4$ (*6*), $Cu_3Mo_2O_9$ (*11, 12*), and $Cu_{4-x}Mo_3O_{12}$ (*13*). X-Ray powder patterns or unit-cell parameters were published also for Cu_2MoO_5 (*8*), $Cu_6Mo_4O_{15}$ (*8*), and $Cu_3Mo_2O_8$ (*10*), but their chemical composition has not been sufficiently confirmed by chemical analysis. As pointed up by Katz *et al.* (*13*) the unit-cell dimensions for $Cu_3Mo_2O_8$ (*10*) and $Cu_{4-x}Mo_3O_{12}$ (*13*) are practically the same but the latter formula fits other structural data much better. Existence of Cu_2MoO_5 has not been confirmed in our previous works (*15–17*). As follows from the X-ray and chemical analyses (including selective dissolution of phases from a multicomponent mixture) Cu_2MoO_5 cannot be synthesized by

0022-4596/80/020135-09$02.00/0

solid state reaction ($2CuO+MoO_3$, 300–650°C) (*15*), by precipitation even with a large excess of the added copper salt (*16, 17*), or by oxidation of previously melted and reduced copper molybdates with or without admixture of CuO (*15*). It can be also observed that the X-ray patterns of Cu_2MoO_5 (*8*) differ from those of $Cu_3Mo_2O_9$ (*8, 11, 12*) only by a slight systematic shift and by their relative intensities, which may be ascribed to preferred orientation of the grains.

In view of the above-mentioned facts we have undertaken systematic studies of the Cu_2O–CuO–MoO_3. system. In the present paper we aim to answer the questions, What is the number and composition of cupric, cuprous, or cuprous–cupric molybdates and what are the structural and physicochemical properties which enable their identification.

Experimental

Cu_2O, CuO, and MoO_3 (all commercial products of p.a. grade) were mixed in different proportions (see Table I) to cover with experimental points the whole area of the triangular diagram. Mixtures of 2 g were placed in 5-ml quartz tubes, sealed after evacuation to 10^{-2} Torr, and heated at 520± 10°C for 10 hr. As follows from preliminary experiments, the temperature of preparation may not be lower if total conversion is required in reasonable time.

Phase composition was determined by powder X-ray analysis at room temperature using a Rigaku–Denki Model D3F diffractometer, CuKα radiation, and CaF_2 ($a = 5.4626$ Å (*18*)) as a reference.

DTA was performed on a Setaram Micro-ATD M-5 apparatus in a stream of argon at heating and cooling rates of 10°C/min. Samples of 25 mg were placed in platinum crucibles and aluminium oxide was used as a reference. The thermal effects were characterized by onset temperatures on heating.

Infrared spectra were recorded with a Fourier type FTS-14 Digilab spectrometer in the range 100–1100 cm^{-1}. The Nujol mull technique was applied for the range 100–450 cm^{-1} and the KBr disk technique for the range 450–1100 cm^{-1}.

Magnetic susceptibility was measured in the temperature range 150–435°K using the Gouy method as described in Ref. (*19*) and tris(ethylenediamine)nickel(II) thiosulfate as calibrant ($10^6 \chi_g = 10.82$ at 25°C) (*20*). As the measured value did not depend on the magnetic field strength (with the exception of $CuMoO_4$ below the Néel temperature), $H =$ 4 kOe was chosen as standard. The correction for the susceptibility of the glass tube was determined experimentally and the diamagnetic corrections were calculated according to Klemm's method (*21*).

Results and Discussion

The results of X-ray phase analysis of the studied samples are summarized in Table I. Identification of Cu_2O, CuO, MoO_3, $CuMoO_4$, $Cu_3Mo_2O_9$, and $Cu_{4-x}Mo_3O_{12}$ was based on the ASTM and literature data quoted in the Introduction. It was found that in addition to the patterns of the six compounds mentioned above, three other groups of diffraction lines appear (see Table II). The reflections characteristic of the first two groups become strongest at the compositions $Cu_2Mo_3O_{10}$ and $Cu_6Mo_4O_{15}$, respectively, and at the same time all foreign peaks disappear. The same is observed for the third group of diffraction lines in the composition range $Cu_{4-x}Mo_3O_{12}$, $0.30 \leq x \leq 0.40$, but this group is always accompanied by the patterns of "normal" $Cu_{4-x}Mo_3O_{12}$ (*13*). The samples of composition $Cu_2Mo_3O_{10}$ and $Cu_6Mo_4O_{15}$ show in DTA (Fig. 1) single, intense, narrow, and reversible peaks at 532 and 466°C, respectively, which may be ascribed to congruent melting of pure compounds. This conclusion has been verified by (1) visual

TABLE I

PHASE COMPOSITION OF THE MIXTURES OF Cu_2O, CuO, AND MoO_3 HEATED AT 520°C FOR 10 hr[a]

Sample number	Mole content of simple oxides in the initial mixture			Phase composition of the product
	Cu_2O	CuO	MoO_3	
1	1	2	3	$\alpha(4-x)$, $\frac{6}{4}$
2	0.95	2.05	3	$\alpha(4-x)$, $\frac{6}{4}$
3	0.90	2.10	3	$\alpha(4-x)$
4	0.85	2.15	3	$\alpha(4-x)$
5	0.80	2.20	3	$\alpha(4-x)$
6	0.75	2.25	3	$\alpha(4-x)$
7	0.70	2.30	3	$\alpha(4-x)$, $\beta(4-x)$
8	0.65	2.35	3	$\alpha(4-x)$, $\beta(4-x)$
9	0.60	2.40	3	$\alpha(4-x)$, $\beta(4-x)$
10	0.35	2.74	3	$\alpha(4-x)$, $\frac{1}{1}$, $\beta(4-x)$
11	0.98	2.55	3	$\alpha(4-x)$, $\frac{3}{2}$
11a	0.98	2.55	3	MoO_3, CuO, Cu_2O, $\frac{6}{4}$, $\frac{3}{2}$
12	0.77	2.44	3	$\alpha(4-x)$, $\frac{3}{2}$
13	0.75	2.32	3	$\alpha(4-x)$, $\beta(4-x)$
14	0.95	1.91	3	$\alpha(4-x)$, $\frac{6}{4}$
15	0.85	1.83	3	$\alpha(4-x)$, $\frac{2}{3}$
16	0.78	1.96	3	$\alpha(4-x)$, $\frac{2}{3}$
17	0.72	2.09	3	$\alpha(4-x)$, $\frac{2}{3}$
18	0.65	2.22	3	$\alpha(4-x)$, $\frac{2}{3}$
19	0.75	1.75	3	$\frac{2}{3}$, $\frac{1}{1}$, $\alpha(4-x)$
20	0.69	1.88	3	$\frac{2}{3}$, $\frac{1}{1}$, $\alpha(4-x)$
21	0.50	2.25	3	$\frac{2}{3}$, $\frac{1}{1}$, $\alpha(4-x)$
22	0.75	3.00	3	$\alpha(4-x)$, $\frac{3}{2}$
22a	0.75	3.00	3	MoO_3, CuO, Cu_2O, $\frac{6}{4}$, $\frac{3}{2}$
23	0.60	1.80	3	$\frac{2}{3}$, $\frac{1}{1}$, $\alpha(4-x)$
24	0.43	1.71	3	$\frac{1}{1}$, $\frac{2}{3}$, MoO_3
24a	0.43	1.71	3	$\frac{1}{1}$, $\frac{2}{3}$
25	0.50	1.00	3	MoO_3, $\frac{2}{3}$, $\frac{1}{1}$
26	0.75	0.75	3	$\frac{2}{3}$, MoO_3, $\frac{1}{1}$
26a	0.75	0.75	3	$\frac{2}{3}$, $\frac{1}{1}$
27	0.60	0.60	3	MoO_3, $\frac{2}{3}$, $\frac{1}{1}$
28	1.00	—	3	$\frac{2}{3}$
29	0.50	—	3	MoO_3, $\frac{2}{3}$
30	1.00	1.00	3	$\frac{2}{3}$, $\alpha(4-x)$
31	2.00	1.00	4	$\frac{6}{4}$, $\alpha(4-x)$
32	2.00	2.00	4	$\alpha(4-x)$, $\frac{6}{4}$
32a	2.00	2.00	4	MoO_3, Cu_2O, CuO, $\frac{6}{4}$, $\frac{3}{2}$
33	2.00	—	4	$\frac{2}{3}$, $\frac{6}{4}$
34	2.67	—	4	$\frac{6}{4}$
35	3.00	—	4	$\frac{6}{4}$
36	4.00	—	4	$\frac{6}{4}$, Cu_2O
37	3.55	7.09	4	Cu_2O, CuO, $\frac{3}{2}$
38	14.00	8.00	4	Cu_2O, $\frac{3}{2}$, CuO
39	4.00	28.00	4	CuO, Cu_2O, $\frac{3}{2}$
40[b]	—	1.00	1	$\frac{1}{1}$
41[b]	—	3.00	2	$\frac{3}{2}$
42[b]	—	2.00	1	$\frac{3}{2}$, CuO

[a] Samples 24a and 26a heated at 520°C for 50 hr; 11a, 22a, and 32a heated at 440°C for 40 hr. $\frac{1}{1}$, $CuMoO_4$; $\frac{3}{2}$, $Cu_3Mo_2O_9$; $\frac{2}{3}$, $Cu_2Mo_3O_{10}$; $\frac{6}{4}$, $Cu_6Mo_4O_{15}$; $\alpha(4-x)$ and $\beta(4-x)$, α- and β-$Cu_{4-x}Mo_3O_{12}$), respectively.

[b] The same products are obtained if the respective mixtures of CuO and MoO_3 are heated in air at 500–650°C (*15*).

observation of samples heated slowly in a vacuum of 10^{-2} Torr in a furnace equipped with quartz window, and (2) X-ray analysis of the quickly cooled melt. On the other hand, if the overall composition of the sample differs from $Cu_2Mo_3O_{10}$ or $Cu_6Mo_4O_{15}$ by several percent in any direction in the diagram, the DTA curves become rich in additional peaks (eutectics or other phenomena). The above-presented results clearly demonstrate that the compounds $Cu_2Mo_3O_{10}$ and $Cu_6Mo_4O_{15}$ actually exist in the system Cu_2O–CuO–MoO_3. The X-Ray patterns of $Cu_6Mo_4O_{15}$ and its melting point found in the present studies differ, however, from those reported in Ref. (*8*).

DTA of $Cu_{4-x}Mo_3O_{12}$ reveals two peaks, the positions of which depend slightly on composition. With x increasing from 0.10 to 0.40 the first of the peaks shifts from 525 to 530°C and the second (visually identified as melting) moves from 650 to 630°C. It was observed also that with x rising above 0.15 the intensity of the first peak, recorded on cooling or on subsequent heating, gradually diminished. In parallel (i.e., for $x > 0.15$) the intensity of the third group of additional X-ray patterns increases. It may be thus concluded that the previously described (*13*) α-$Cu_{4-x}Mo_3O_{12}$ has a high-temperature β polymorph stable above ~525°C, the $\beta \rightarrow \alpha$ transformation being inhibited at the lower copper content in this nonstoichiometric

TABLE II

X-RAY PATTERNS OF $Cu_2Mo_3O_{10}$, $Cu_6Mo_4O_{15}$ AND β-$Cu_{4-x}Mo_3O_{12}$[a]

$Cu_2Mo_3O_{10}$		$Cu_6Mo_4O_{15}$		β-$Cu_{4-x}Mo_3O_{12}$	
d(Å)	I	d(Å)	I	d(Å)	I
8.18	vw				
8.06	w			8.10	m
				7.01	m
6.57	vw				
6.27	vw				
		5.77	m		
5.59	vw				
5.18	vw				
				5.08	vw
		4.69	vw	4.54	vw
		4.38	vw		
4.33	w				
4.06	vw				
				4.02	m
3.93	ms				
		3.89	vw	3.91	ms
				3.86	m
		3.80	vw		
3.74	vw	3.72	vw		
3.64	vw	3.63	w		
		3.53	vw	3.52	m
3.42	w	3.42	vw		
3.39	vw				
3.22	m			3.24	w
3.18	m	3.18	ms	3.17	vs
3.15	m				
3.10	m				
3.08	vw			3.07	m
3.01	vs	3.02	w		
2.988	vs	2.974	vs		
		2.947	m		
		2.913	s		
2.892	vw	2.889	m		
2.879	w				
2.811	vw				
2.798	w				
2.789	w				
		2.696	ms		
		2.630	vw	2.61	w
2.566	w				
		2.534	w		

[a] Cu$K\alpha$ radiation, CaF_2 as a reference. vs, very strong; s, strong, ms, middle strong; m, middle; w, weak; vw, very weak.

compound. It appears also from DTA and X-ray analyses (Table I, samples 2–9) that the discussed phase may exist over a wide range of composition, i.e., $0.10 \leq x \leq 0.40$.

The results of DTA and TG analyses of $CuMoO_4$ and $Cu_3Mo_2O_9$ will be discussed in detail in a forthcoming paper dealing with the CuO–MoO_3 phase diagram. Here we would like to mention only that they melt in air at 820 and 855°C, respectively, with simultaneous decomposition (oxygen loss); in the stream of argon their temperatures of decomposition and melting are lowered to 745°C ($CuMoO_4$) and 760°C ($Cu_3Mo_2O_9$).

For more profound characterization of the phases appearing in the system Cu_2O–CuO–MoO_3 ir spectra were recorded and magnetic susceptibility was measured.

Infrared spectra of $CuMoO_4$, $Cu_3Mo_2O_9$, $Cu_2Mo_3O_{10}$, $Cu_6Mo_4O_{15}$, and $Cu_{4-x}Mo_3O_{12}$ are shown in Fig. 2. At present they are regarded only as a "fingerprint" useful for phase identification.

Magnetic susceptibility measurements are summarized in Table III and in Fig. 3. The results obtained for $Cu_2Mo_3O_{10}$ and $Cu_6Mo_4O_{15}$ suggest the presence of $Cu^+(3d^{10})$ and $Mo^{6+}(4s^2p^6)$ diamagnetic ions, the participation of covalent bonding being apparently responsible for the weak temperature-independent paramagnetism. $Cu_3Mo_2O_9$ (above 150°K) and $CuMoO_4$ (above $T_N = 200$°K) are paramagnetics, obeying the Curie–Weiss law. The μ_{eff} values of 1.71 and 1.80 B.M. approach closely the spin-only magnetic moment of Cu^{2+} $(3d^9)$ ions. $Cu_{4-x}Mo_3O_{12}$ is also paramagnetic but the calculated μ_{eff} values strongly depends on the assumptions concerning the valence state of the cations, participation of molybdenum in the paramagnetism, and to some extent on the method of determination of diamagnetic corrections. For illustration we have inserted in Table III the values of μ_{eff} obtained under the assumption that Cu^{2+} ions alone are responsible for the paramag-

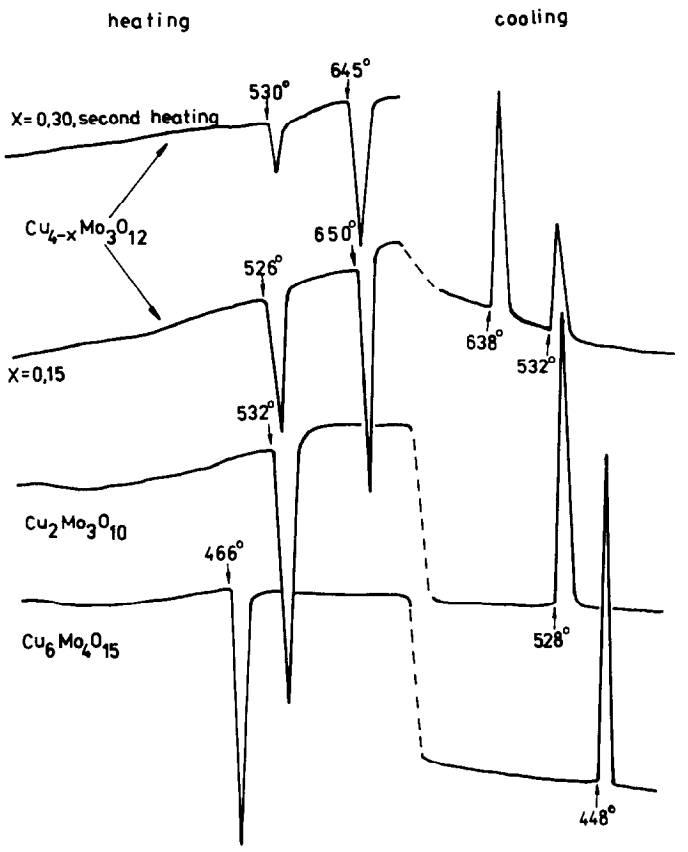

FIG. 1. DTA curves of $Cu_2Mo_3O_{10}$, $Cu_6Mo_4O_{15}$, and $Cu_{4-x}Mo_3O_{12}$ recorded in argon.

netism and the contribution of molybdenum in paramagnetism may be neglected (it was taken into account that the oxides MoO_3, MoO_2, and a sample with intermediate composition referred to as "Mo_2O_5" (*22*) show very weak temperature-independent paramagnetism even if some of them formally contain paramagnetic ions). As seen the most reasonable value of μ_{eff} has been found for the valence composition $Cu_{4-x}Mo_3O_{12} = Cu_3^{2+}Cu_{1-x}^{0}Mo_3^{6+}O_{12}$. As, however, the magnetic susceptibility measurements may not finally resolve the problem of the valency of copper, photoelectron spectroscopy studies were performed (*23*) which brought decisive arguments for the correctness of the above mentioned formula.[1] The presence of zerovalent copper in the discussed compound becomes less surprising if we take into account the fact that in its structure (*13*)

[1] Argumentation presented in Ref. (*23*) is based on the fact that the $Cu2p_{3/2}$ binding energy strongly depends on the valence state of copper and is equal to 934.7 eV for Cu^{2+} in $CuMoO_4$ and $Cu_3Mo_2O_9$, 932.2 eV for Cu^+ in $Cu_2Mo_3O_{10}$ and $Cu_6Mo_4O_{15}$, and 933.1 eV for metallic copper. A sample of $Cu_{4-x}Mo_3O_{12}$ ($x = 0.15$) showed a $Cu2p_{3/2}$ doublet of intensity ratio 1 : 3 and binding energy values of 933.1 and 934.7 eV. At the same time a $Mo3d_{7/2}$–$Mo3d_{5/2}$ doublet for $Cu_{4-x}Mo_3O_{12}$ corresponded to the be values of 232.7 and 236.1 eV, which were practically the same as those found for Mo^{6+} in MoO_3 (232.8 and 236.0 eV). Thus the results obtained fit the formula $Cu_3^{2+}Cu_{1-x}^{0}Mo_3^{6+}O_{12}$.

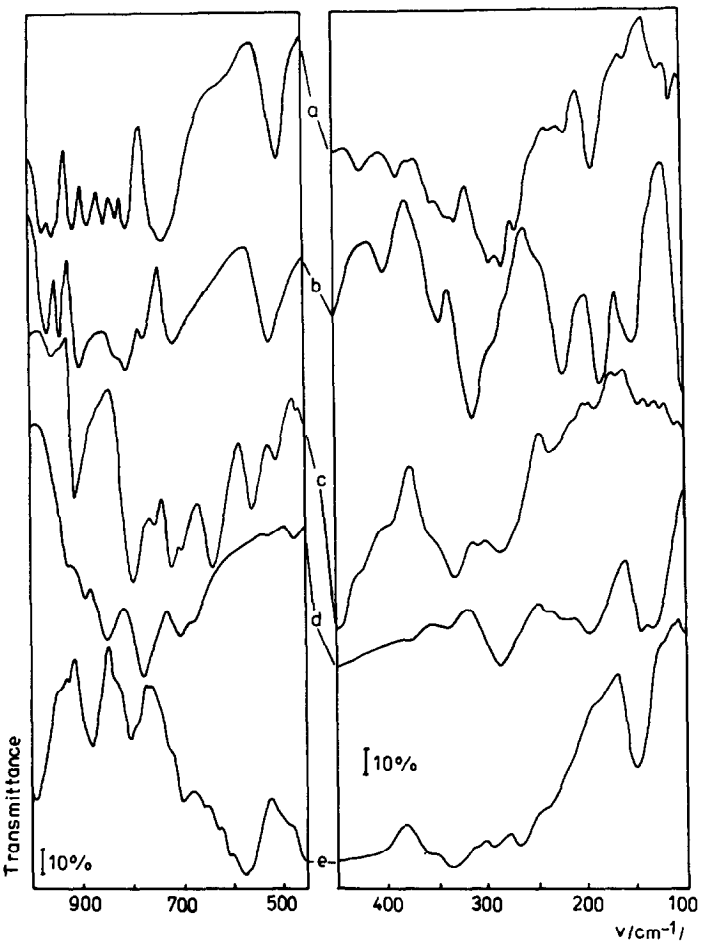

FIG. 2. Infrared spectra of copper molybdates. (a) $CuMoO_4$; (b) $Cu_3Mo_2O_9$; (c) $Cu_6Mo_4O_{15}$; (d) $Cu_{4-x}Mo_3O_{12}$; (e) $Cu_2Mo_3O_{10}$.

some copper atoms $(1-x)$ are localized in chains of face-sharing octahedra with Cu–Cu distances across the face equal to 2.51 Å, which is even less than that in metallic copper (2.556 Å).

On the basis of the results obtained the subsolidus phase diagram of the system Cu_2O–CuO–MoO_3 has been constructed (Fig. 4). The indexed points represent the overall composition of all samples studied (Table I). The solid dots mark the identified chemical compounds, and the broken lines border the areas of coexistence of the respective phases. It should be added that in some cases (samples 24 and 26) the standard time of the preparation reaction (10 hr at 520°C) was not sufficient for their completion, but the total conversion was reached after prolonged heating (samples 24a and 26a). In some other cases (samples 11, 22, and 32) the preparations were already melted at 520°C and the phase composition of the product was apparently inconsistent with the diagram due to the influence of crystallization equilibria frozen at room temperature (this phenomenon will be discussed in detail in the forthcoming paper). In view of this fact the above-mentioned three samples were pre-

TABLE III

MAGNETIC PROPERTIES OF COPPER MOLYBDATES

Sample	Temp. range (°K)	$\chi_g \times 10^6$ at 293°K	μ_{eff} (B.M.)	θ (°K)	Néel temp. (°K)
$CuMoO_4$	150–415	6.80	1.80	28	200
$Cu_3Mo_2O_9$	150–410	6.77	1.71	−12	—
$Cu_6Mo_4O_{15}$	150–300	0.64	Weak temperature-independent paramagnetism		
$Cu_2Mo_3O_{10}$	150–300	0.55	Weak temperature-independent paramagnetism		
$Cu_{4-x}Mo_3O_{12}$ ($x = 0.15$)	150–435	4.06		−93	—
Assumed valence composition of metals					
(a) $3Cu^{2+} + 0.85Cu^0 + 3Mo^{6+}$			1.74		
(b) $2.15Cu^{2+} + 1.70Cu^{+} + 3Mo^{6+}$			2.06		
(c) $3.85Cu^{2+}$ + respective amount of Mo^{6+} and Mo^{5+} or Mo^{4+}			1.54		

pared again at a lower calcination temperature of 440°C (subsolidus range). In agreement with the diagram $Cu_6Mo_4O_{15}$ and $Cu_3Mo_2O_9$ were identified as the reaction products; however, due to kinetic hindrances the samples contained a fair amount of unreacted simple oxides.

Finally we would like to add that in the same manner the area of the triangle Cu_2O–MoO_2–MoO_3 has been examined, but no new phase has been found.

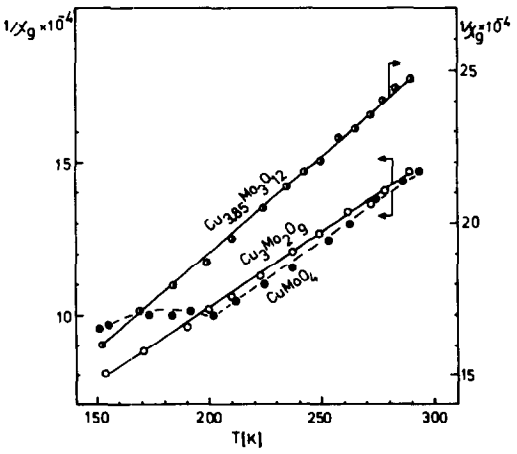

FIG. 3. Magnetic susceptibility of $CuMoO_4$, $Cu_3Mo_2O_9$, and $Cu_{4-x}Mo_3O_{12}$ ($x = 0.15$) as a function of temperature.

Conclusions

There are five chemical compounds existing in the Cu_2O–CuO–MoO_3 system, i.e., $CuMoO_3$ (pale green), $Cu_3Mo_2O_9$ (snuff colored), $Cu_2Mo_3O_{10}$, $Cu_6Mo_4O_{15}$, and $Cu_{4-x}Mo_3O_{12}$ ($0.10 \leq x \leq 0.40$) (all black).

Cupric molybdates $CuMoO_4$ and $Cu_3Mo_2O_9$ melt with simultaneous decomposition (oxygen loss) at 820 and 855°C in air or at 745 at 760°C in argon, respectively. $Cu^{2+}(3d^9)$ ions show in both compounds an effective magnetic moment approaching the spin-only value (Table III). Below 200°K, $CuMoO_4$ becomes antiferromagnetic. The powder X-ray patterns of cupric molybdates studied in the present paper agree with the data of previous papers (*5, 11, 12*) in which their structures were solved.

Cuprous molybdates $Cu_2Mo_3O_{10}$ and $Cu_6Mo_4O_{15}$ melt congruently in argon at 532 and 466°C, respectively. Both show weak temperature-independent paramagnetism. For their identification, X-ray powder

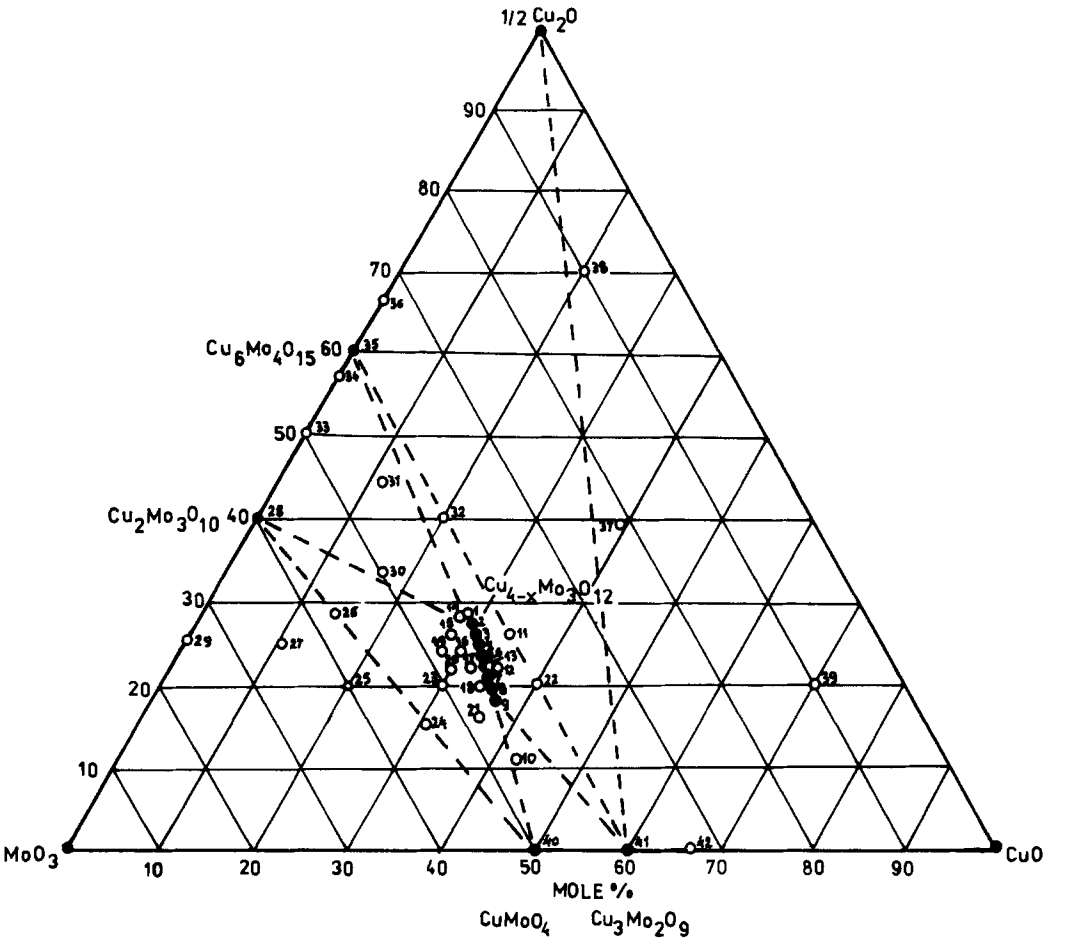

FIG. 4. Subsolidus phase diagram of the Cu_2O–CuO–MoO_3 system.

patterns which are presented in Table II may be used.

There is only one nonstoichiometric compound, $Cu_{4-x}Mo_3O_{12}$, which formally may be placed inside the triangular diagram Cu_2O–CuO–MoO_3, but its real valence composition is described by the formula $Cu_3^{2+}Cu_{1-x}^{0}Mo_3O_{12}$. Cu^{2+} ions show in this compound $\mu_{eff} = 1.74$ B.M. Depending on x, $Cu_{4-x}Mo_3O_{12}$ melts congruently in argon between 630 and 650°C and at 525–530°C undergoes polymorphic transformation to the high-temperature β modification. The reverse transformation $\beta \rightarrow \alpha$ is inhibited at low copper content. Low-temperature α-$Cu_{4-x}Mo_3O_{12}$ shows X-ray powder patterns which agree with earlier structure determinations (*13*); the β form may be identified using the data in Table II.

Infrared spectra of all five compounds, though not yet interpreted in detail, show evident differences between the dynamics of their chemical bonds.

Acknowledgments

The authors wish to express their sincere thanks to Professor J. Haber for his interest and helpful discussions. Thanks are due also to Dr. T. Romotowski and to Dr. M. Handke from the Regional Laboratory of Physicochemical Analyses and Structural Research in Cracow for assistance at registration of ir spectra.

References

1. A. N. ZELIKMAN AND L. V. BELYAEVSKAYA, *Zh. Prikl. Khim.* **27**, 1151 (1954).
2. A. N. ZELIKMAN, *Zh. Neorg. Khim. Leningrad*, **1**, 2778 (1956).
3. N. A. BATRAKOV, *Sklar. Keram.* **12**, 147 (1962).
4. W. P. DOYLE, G. MCGUIRE, AND G. M. CLARK, *J. Inorg. Nucl. Chem.* **28**, 1185 (1966).
5. R. KOHLMULLER AND J. P. FOURIE, *C. R. Acad. Sci. Paris* **264**, 1151 (1967).
6. S. C. ABRAHAMS, J. L. BERNSTEIN, AND P. B. JAMIESON, *J. Chem. Phys.* **48**, 2619 (1968).
7. K. NASSAU AND S. C. ABRAHAMS, *J. Crystal Growth* **2**, 136 (1968).
8. K. NASSAU AND J. W. SHIEVER, *J. Amer. Ceram. Soc.* **52**, 36 (1969).
9. E. V. TKATCHENKO, V. M. ZHUKOVSKII, AND T. E. TYLNYKH, *Zh. Fiz. Khim.* **49**, 809 (1975).
10. I. D. THOMAS, A. H. HERZOG, AND D. MCLACHLAN, *Acta Crystallogr.* **9**, 316 (1956).
11. L. KIHLBORG, R. NORRESTAM, AND B. OLIVECRONA, *Acta Crystallogr. Sect. B* **27**, 2066 (1971).
12. L. KIHLBORG AND R. NORRESTAM, *Acta Crystallogr. Sec. B* **28**, 3097 (1972).
13. L. KATZ, A. KASENALLY, AND L. KIHLBORG, *Acta Crystallogr. Sect. B* **27**, 2071 (1971).
14. I. D. THOMAS, Ph.D. thesis, University of Utah (1961) (quoted in (*8*)).
15. T. MACHEJ AND J. ZIÓŁKOWSKI, *Bull. Acad. Pol. Sci. Ser. Sci. Chim.* **24**, 577 (1976).
16. T. MACHEJ AND J. ZIÓŁKOWSKI, *Bull. Acad. Pol. Sci. Ser. Sci. Chim.* **24**, 455 (1976).
17. T. MACHEJ, T. ROMOTOWSKI, AND J. ZIÓŁKOWSKI, *Bull. Acad. Pol. Sci. Ser. Sci. Chim.* **25**, 467 (1977).
18. Joint Committee of Powder Diffraction File 4-864.
19. L. DZIEMBAJ AND J. ZIÓŁKOWSKI, *Bull. Acad. Pol. Sci. Ser. Sci. Chim.* **20**, 725 (1972).
20. N. F. CURTIS, *J. Chem. Soc.*, 3147 (1961).
21. P. W. SELWOOD, "Magnetochemistry," p. 78, Interscience, New York/London (1956).
22. I. K. KIKONIN, "Tablitsy Fizitcheskikh velitchin," Atomizdat, Moscow (1976).
23. J. HABER, T. MACHEJ, L. UNGIER, AND J. ZIÓŁKOWSKI, *J. Solid State Chem.* **25**, 207 (1978).